AD-A283 323

OXIDATION RESISTANT COATING FOR CARBON-CARBON COMPOSITES AT ULTRA-HIGH TEMPERATURES

FINAL REPORT

Contract N00014-92-C-0049

DISTRIBUTION STATEMENT A
Approved for public release;
Distribution Unlimited

J. Paul Pemsler and John K. Litchfield
Castle Technology Corpration
Lexington, MA

and

Richard Cooke and Mark Smith
Surmet Corporation
Burlington, MA

DTIC
ELECTE
AUG 0 3 1994
S B D

DTIC QUALITY INSPECTED 2

94-17795

June 1, 1994

94-24412

94 6 9 075

94 8 02 094

SUMMARY

A novel coating to protect carbon-carbon composites (C-C) from oxidation at temperatures as high as 1600°-2000°C was investigated. The duplex coating consists of 1) an inner diffusion barrier of carbon fiber reinforced iridium or rhodium and 2) an outer layer of plasma sprayed lanthanum hafnate.

The diffusion barrier was produced by electrochemically infiltrating noble metal into a specially prepared surface zone of C-C to produce a **CA**rbon **F**iber **R**einforced **I**nternal **B**arrier (**CAFRIB**). The **CAFRIB** configuration acts as a near total diffusion block to both oxygen transport inward and carbon transport outward. **CAFRIB** also serves to withstand the large stresses resulting from the thermal expansion mismatch between C-C and the coating.

Matrix carbon char was quantitatively removed from surface layers of two-dimensional C-C by oxidation at controlled temperature and oxygen pressure. Carbon fibers are not attacked by the process. The resulting matrix-free woven fiber surface layer, typically 30 micrometers in depth, served as host for the **CAFRIB** layer.

Efforts to prepare iridium-infiltrated **CAFRIB** by electrodeposition of metal into the matrix-free layer were only partially successful. Iridium deposited from a molten salt bath penetrated to about 10 micrometers. Iridium deposited from an aqueous bath adequately penetrated the **CAFRIB** region but was highly cracked.

Rhodium-infiltrated **CAFRIB** was successfully formed from an aqueous electrolyte. Periodic current reversal techniques were used during the electrodeposition to fill the matrix-free layer with rhodium.

Thermal cycling studies of rhodium **CAFRIB** to 1400°C and 1600°C indicate that the **CAFRIB** layer exhibits greatly improved coating adherence and crack resistance compared with rhodium plated onto conventional C-C. However, due to the non-wetting of carbon fibers by rhodium, the **CAFRIB** layer destabilizes internally at high temperatures when rhodium debonds from the fibers to form tiny rhodium spheres. Carbon fiber surfaces need to be modified so that they are wet by noble metals to ensure stability of the **CAFRIB** configuration.

The outer ceramic coating minimizes erosion and vaporization loss of the **CAFRIB** layer. Lanthanum hafnate of controlled porosity was successfully deposited on both rhodium and iridium barrier layers by plasma spraying. A co-precipitated mixed oxide of lanthanum and hafnium, used as the powder feed, reacted during plasma spraying to form the desired lanthanum hafnate coating.

Accession For
NTIS GRA&I ☑
DTIC TAB ☐
Unannounced ☐
Justification
By per letter
Distribution/
Availability Codes
Avail and/or
Dist Special
A-1

TABLE OF CONTENTS

1. INTRODUCTION....1

1.1 Background....1
1.2 Composites for Very High Temperature Use....1
1.3 Coating Requirements....2
1.4 The 2000°C Problem....2
1.5 Hafnia-Based Coatings....3
1.6 Diffusion Barrier Requirements....4
1.6.1 Barrier Materials....4
1.6.2 Bonding to Carbon- Carbon Composites....5
1.6.3 Vaporization Losses....5
1.6.4 Thermal Expansion Mismatch....6
1.7 Castle Technology Coating System....8

2. LANTHANUM HAFNATE OUTER LAYER....10
2.1 Preparation of Powder Feed....10
2.2 Plasma Spraying of Lanthanum Hafnate....14
2.2.1 Coating Methodology....14
2.2.2 Plasma Spray Results....16
2.3 Plasma Coating Lanthanum Hafnate on Iridium....21

3. CAFRIB INNER BARRIER LAYER....22
3.1 Carbon-Carbon Composite Material....22
3.2 Preparation of Matrix-Free Zone....22
3.2.1 Reactive Ion Etching....23
3.2.2 Anodic Oxidation....24
3.2.3 Thermal Oxidation....25
3.3 Electrochemical Impregnation....31
3.3.1 Previous Studies....31
3.3.2 Molten Salt Electrodeposition of Iridium....32
3.3.3 Aqueous Deposition of Iridium....36
3.3.4 Aqueous Deposition of Rhodium....38
3.3.5 Duplex Rhodium/Iridium Barrier....41

4. THERMAL CYCLING STUDIES....42

5. CONCLUSIONS....46

6. REFERENCES....47

7. ACKNOWLEDGEMENT....48

1. INTRODUCTION

1.1 Background

Significant advances have been made during the last several decades in the development of materials for high temperature service in aerospace missions. Metal alloys, ceramics and composites have each found a place in the various structural and engine components subject to high temperature oxidizing atmospheres. The desire to extend vehicle performance in both military and civilian applications poses challenges considerably beyond the capabilities of even the most advanced systems currently in use.

1.2 Composites for Very High Temperature Use

Only a limited number of materials are capable of surviving an operating temperature of 2000°C in an oxidizing atmosphere. Several composites appear to possess the intrinsic strength-to-weight ratio and high temperature stability to serve as structural materials. These include carbon or refractory carbide fibers in a carbon matrix, and several simple or mixed oxide fibers in an oxide matrix. Carbon-carbon composites (C-C) have extensive technological development, diverse manufacturing techniques and potentially low cost.

Coatings for C-C are currently based on a complex series of layers each of which is designed to fulfill a role in providing overall protection. Oxidation protection is ultimately based on a protective layer of SiO_2. However, SiO_2 reacts with carbon and carbides to form carbon monoxide and loses SiO species by vaporization below the temperature required for improved engine operation. Even the most advanced coatings based on silica or refrac-

tory silicates will be unable to protect C-C at 1600-2000°C.

1.3 Coating Requirements

In order to protect C-C composites at 1600-2000°C, a number of features must be addressed which are also common to lower temperature coating systems: 1) oxidation of the underlying composite must be prevented, 2) the coating and substrate must be chemically compatible so that degradation by interdiffusion does not undermine the protective feature of the coating or structural integrity of the substrate, 3) adherence to the substrate must be maintained both isothermally and during thermal cycling, 4) the coating must resist vaporization losses for extended periods of time, and 5) the coating must have adequate mechanical properties.

1.4 The 2000°C Problem

The list of materials which can serve as resistant coatings narrows appreciably at 2000°C. Although a substantial number of oxides, carbides, nitrides, sulfides and intermetallics have melting points in excess of 2000°C, very few have the ability to withstand high vaporization losses in air at that temperature. Hafnium oxide, HfO_2, is especially suited to this task. The loss in free evaporation of HfO_2 is calculated from vapor pressure data (1) to be 0.4 um in 1000 hrs at 1600°C, 2.4 um in 1000 hrs at 1800°C and 6.3 um in 1000 hrs at 2000°C. It is reasonable, then, to look toward HfO_2-based materials as the outer layer in a coating system designed for extended performance at 2000°C.

The problem of thermal expansion mismatch of coating and substrate is especially severe when one considers both that the coefficient of thermal expansion of HfO_2 is about nine times

greater than that of C-C and that the coating must remain in place from below 0° to $2000^{o}C$.

Another feature of great importance is that somewhere within the coating system there must be a layer which will prevent oxidation of the C-C composite. That is, there must be a barrier to control the migration of oxygen inward and the diffusion of carbon outward. While HfO_2 is suitable as an outer layer coating, it has a significant concentration of mobile oxygen ion vacancies at elevated temperature and is, therefore, unlikely to adequately prevent oxygen access to the carbon substrate.

1.5 Hafnia-Based Coatings

The properties of several rare earth-hafnium oxide compounds are extremely attractive and, as yet, largely unexplored. In previous studies (2,3) Castle Technology investigated those rare earth hafnates which have pyrochlore structures. Phase equilibria for the rare earth subset La_2O_3, Pr_6O_{11}, Nd_2O_3, Sm_2O_3, Gd_2O_3 and Tb_2O_3 - HfO_2 compounds based on the composition $Ln_2Hf_2O_7$ were reported by Shevchenko et. al. (4,5). They were found to have a pyrochlore structure and fairly wide ranges of homogeneity (62-72 m/o HfO_2). The phase diagram of the La_2O_3-HfO_2 system is shown in Figure 1.1.

The ordered pyrochlore compound is stable without phase change from room temperature to its melting point at about $2400^{o}C$. Our studies have shown that the pyrochlore structure is retained both after slow cooling and oil quenching from $1600^{o}C$ and that vaporization losses are extremely low in air at 1600 - $2000^{o}C$. The coefficient of thermal expansion of $La_2Hf_2O_7$ is reported as $9 \times 10^{-6}/^{o}C$ (6).

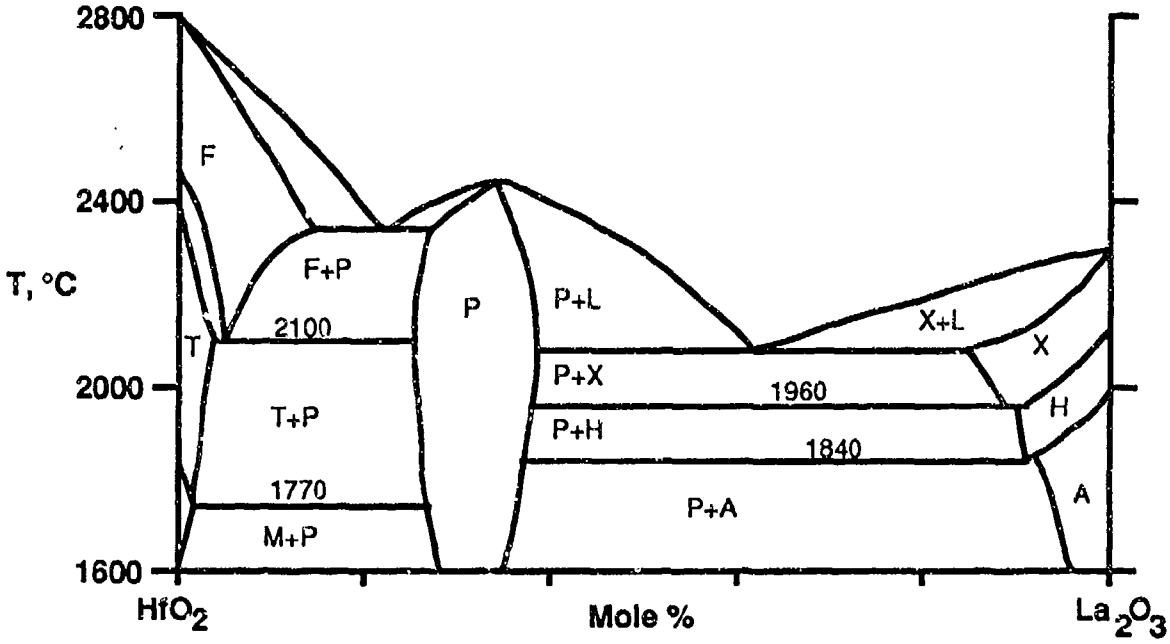

Figure 1.1 Phase Diagram of HfO_2-La_2O_3.

1.6. Diffusion Barrier Requirements

1.6.1 Barrier Materials

Since pyrochlore hafnates are not adequate barriers to oxygen diffusion, and, in any case, would react with carbon to form carbides, oxycarbides and carbon monoxide, it is necessary to provide a diffusion barrier at the coating/carbon-carbon interface.

Iridium and rhodium are the best known barriers to oxygen penetration at very high temperatures. These metals also have extremely low solubility of carbon and function as barriers to

the outward diffusion of carbon. The eutectic temperature in the carbon-iridium system is reported to be 2296°C and in the rhodium-carbon system to be 1694°C. These temperatures, therefore, define the upper bounds of operation for iridium and rhodium barrier layers. Since it has a higher temperature of operation, iridium is the preferred barrier metal.

There are several problems associated with the use of iridium as a diffusion barrier: it is difficult to obtain a good bond to the carbon substrate; vaporization losses in oxidizing atmospheres are unacceptable; and there is a large thermal expansion mismatch between iridium and C-C.

1.6.2 Bonding to Carbon-Carbon Composites

Castle Technology has developed a method for electroplating highly adherent, pore-free iridium coatings onto carbon from a molten halide bath at 580°C (2). In a pull test an iridium-plated graphite specimen failed at 1600 psi parallel to the iridium/graphite interface and within the graphite substrate demonstrating that the interface was stronger than 1600 psi. Therefore, molten salt deposition appears to be a satisfactory method of bonding iridium to carbon.

1.6.3 Vaporization Losses

The unacceptably high rate of loss of iridium by volatile oxide formation can be controlled by coating it with a low volatility oxide. A lanthanum hafnate coating of 50-150 um would create a thick stagnant boundary layer which would greatly retard the diffusion limited loss due to oxidative vaporization. In the fiber glass industry, protective coatings of stabilized zirconia are used to minimize the rate of platinum oxide evaporation.

Studies at Battelle Pacific Northwest Laboratories have shown that a porous coating of zirconia reduces the rate of iridium oxide vaporization by at least an order of magnitude (7).

1.6.4 Thermal Expansion Mismatch

A significant technical problem associated with the use of iridium as a coating on C-C is illustrated in Figure 1.2, which graphically depicts the large difference in the coefficients of thermal expansion (CTE) between the two materials.

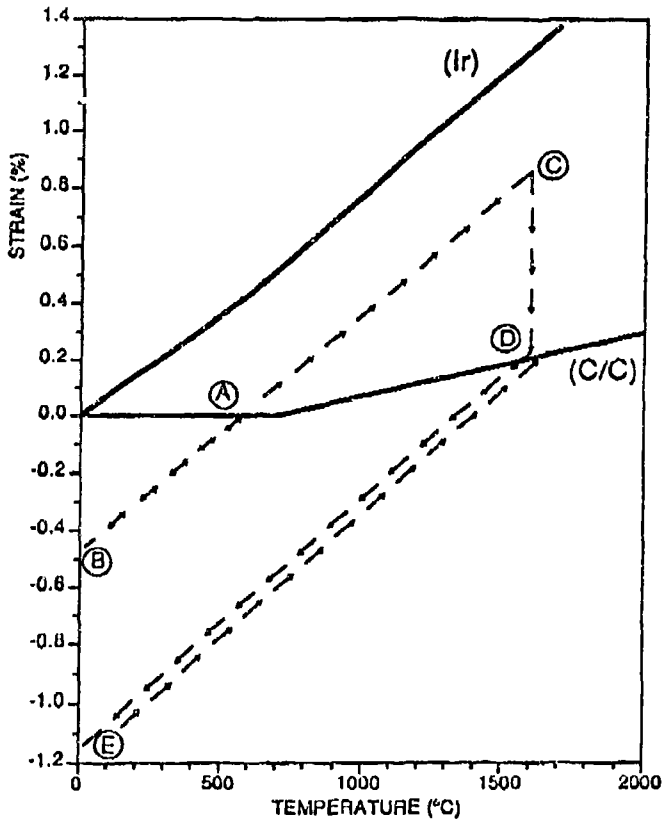

Figure 1.2 Comparison of Linear Thermal Expansion of a C-C composite with iridium. (Dashed lines represent a loading path subsequent to deposition at 580°C.)

The CTE shown for C-C is an idealized curve which implies that the coefficient from room temperature to about 700°C has a value of zero (actually it is slightly negative). Above 700°C,

the average expansion coefficient is $2.3 \times 10^{-6}/^{o}C$. This value is an average because C-C composites are highly anisotropic. For example, the thermal expansion of yarn bundles is negative along the longitudinal axis, but positive in the transverse direction (8). The CTE of the pyrolyzed carbon matrix is less than the transverse expansion of the fiber, but positive and isotropic. Consequently, the finished composites are almost always micro-cracked after fabrication. In comparison, the average CTE for iridium over the temperature range room temperature - 1600°C is about $8.7 \times 10^{-6}/^{o}C$.

If iridium is electroplated onto the surface of a C-C composite at 575-590°C, tensile stresses will develop on subsequent cooling to room temperature as shown by the curve A-B in Figure 1.2. The resultant tensile strain imposed on the iridium coating will be about 0.45%. Given that the modulus of elasticity of iridium is about 500 GPA, this will impose a stress near the yield point. Upon subsequent heating to 1600-2000°C, any tensile cracks that develop in the coating will reclose above the original deposition temperature and the coating will go into compression following the curve B-A-C. The induced stresses are now sufficient to cause buckling but, since iridium exceeds its ductile/brittle transition at 700C, it will become plastic and able to accomodate the imposed strain. In fact, stress relaxation may occur so that the coating follows the path C-D to match the C-C substrate. This will impose an even greater tensile strain (~1.2%) upon return to room temperature along path D-E, and cracking may then occur.

1.7 Castle Technology Coating System

The Castle Technology Coating system for C-C for use at temperatures as high as 1600-2000°C consists of: 1) an inner diffusion barrier of carbon fiber reinforced iridium and 2) an outer coating of plasma sprayed lanthanum hafnate.

In order to accommodate the large tensile stresses, Castle Technology conceived the novel approach of infiltrating iridium into the carbon fibers of a specially prepared surface ply of the C-C composite. This **CA**arbon **R**einforced **I**nternal **D**iffusion **B**arrier, termed **"CAFRIB"**, is illustrated in Figure 1.3.

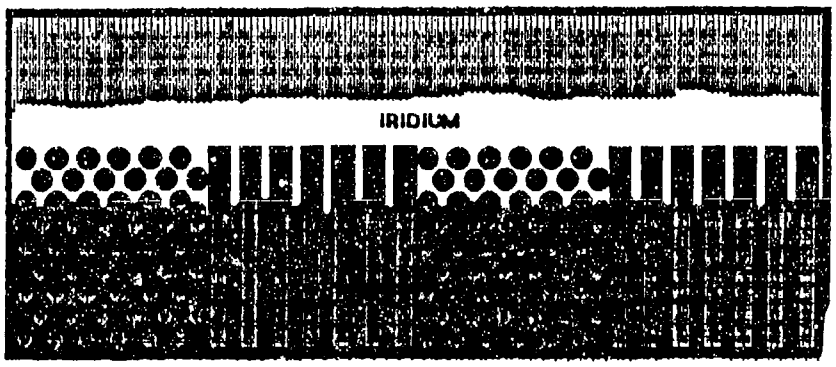

Figure 1.3 Schematic Diagram of the **CAFRIB** Configuration.

Carbon fibers have a much higher strength than iridium and the induced stress resulting from thermal cycling is transferred from the iridium matrix to the carbon fiber through the "shear lag" concept of fiber reinforcement (9). This principle has been widely demonstrated in continuous fiber reinforced metal matrix composites. The more ductile, lower strength, matrix transfers load through rheological interaction at the matrix/fiber interface, thereby allowing the higher strength fiber to carry the

load. Two additional conditions are necessary to achieve composite strengthening: 1) a sufficiently large length/diameter aspect ratio for the fiber (normally the L/D has to be greater than ten), and 2) the absence of chemical bonding at the interface. Both of these conditions are satisfied in an iridium infiltrated carbon fiber coating.

At lower temperatures (e.g. <600°C), iridium may act more like a brittle material and the composite system will become more like a fiber reinforced or ceramic matrix composite. These brittle matrix composites have been shown to exhibit toughness if the interface between fiber/matrix is not chemically bonded. Cracks will deflect along the interface when the interface energy is high relative to the surface energy (10), and the tractions imposed by debonded fibers in the crack wake can be sufficient to arrest the propagating crack (11,12). These effects prevent microcracking in the coating that would lead to exposure of the underlying carbon surface. The carbon reinforced iridium layer remains adherent and is able to accommodate the stresses induced by severe thermal cycling, thereby maintaining oxidation protection.

The behavior of lanthanum hafnate during thermal expansion must also be considered. Since the CTEs of iridium ($8.6 \times 10^{-6}/^{\circ}C$) and lanthanum hafnate ($\sim 9 \times 10^{-6}/^{\circ}C$) are nearly identical, and since the stress due to thermal mismatch with C-C is borne by the carbon fibers in **CAFRIB**, the lanthanum hafnate outer layer should not experience significant stress at the iridium/lanthanum hafnate interface.

2. LANTHANUM HAFNATE OUTER LAYER

2.1 Preparation of Powder Feed

The lanthanum hafnate outer coating was applied by plasma spraying. Powder feed for plasma spraying was prepared by co-precipitation of hafnium and lanthanum salts from a stoichiometric solution. According to the Pourbaix diagrams (11), hafnium hydroxide will precipitate between a pH of 4 and 7, while lanthanum hydroxide will precipitate between a pH of 6 and 10. Therefore, as the pH in the La-Hf solution is increased by addition of NH_4OH, $Hf(OH)_4$ will precipitate first, followed by $La(OH)_3$. By maintaining a low solids density and using rapid stirring, the $Hf(OH)_4$ may precipitate seed particles around which the $La(OH)_3$ will subsequently precipitate to form the stoichiometric fine particulate mixed hydroxide.

The midpoint of the pyrochlore phase field was chosen to give maximum allowances for compositional errors. Hafnium chloride was obtained from Teledyne Wah Chang (Albany, OR) as the sublimed, low-zirconium grade and contained 0.12% zirconium. Lanthanum nitrate was obtained from Unocal Molycorp (White Plains, NY) and contained <1% cerium.

A flow chart for the preparation of powder is shown in Figure 2.1.

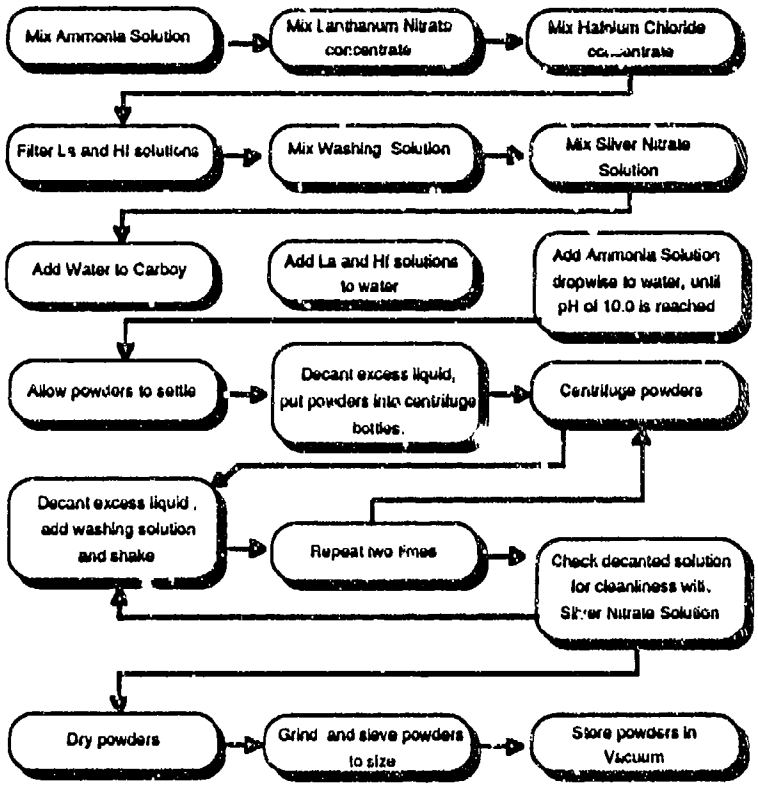

Figure 2.1 Flow chart for the preparation of lanthanum hafnate powder precursor.

Co-precipitation was done using the following procedure:

1. Hafnium chloride and lanthanum nitrate solutions were mixed together and diluted to 0.1M total metals.

2. A 2.5M solution of ammonia was added dropwise with rapid stirring until a pH ~10 was reached.

3. A small amount of ethyl alcohol was added to the turbid solution which was then centrifuged at 3000 rpm for 20 min.

4. Liquid was decanted and the powder redispersed in ammonia-15v/o EtOH with a pH= 11. After centrifuging, the liquid was decanted.

5. Two additional washes in ammonia-EtOH were performed.

6. After the third wash, the solution was tested for residual chloride ions. If the test was positive for either

ion, washing was repeated. Cleaned powder was dispersed in EtOH and oven dried at 120°C for 24 hrs.

Two variations in the next step were used:

7a. The powder was calcined for 8 hrs at 650°C to convert to the mixed oxides and fired at 1100°C in air to form lanthanum hafnate, or

7b. The unreacted mixed oxides were dried at 250°C.

The X-ray diffraction pattern of powder from 7a. is shown in Figure 2.2 and a comparison of two-theta values and intensity with standard powder diffraction patterns is shown in Table 1 .

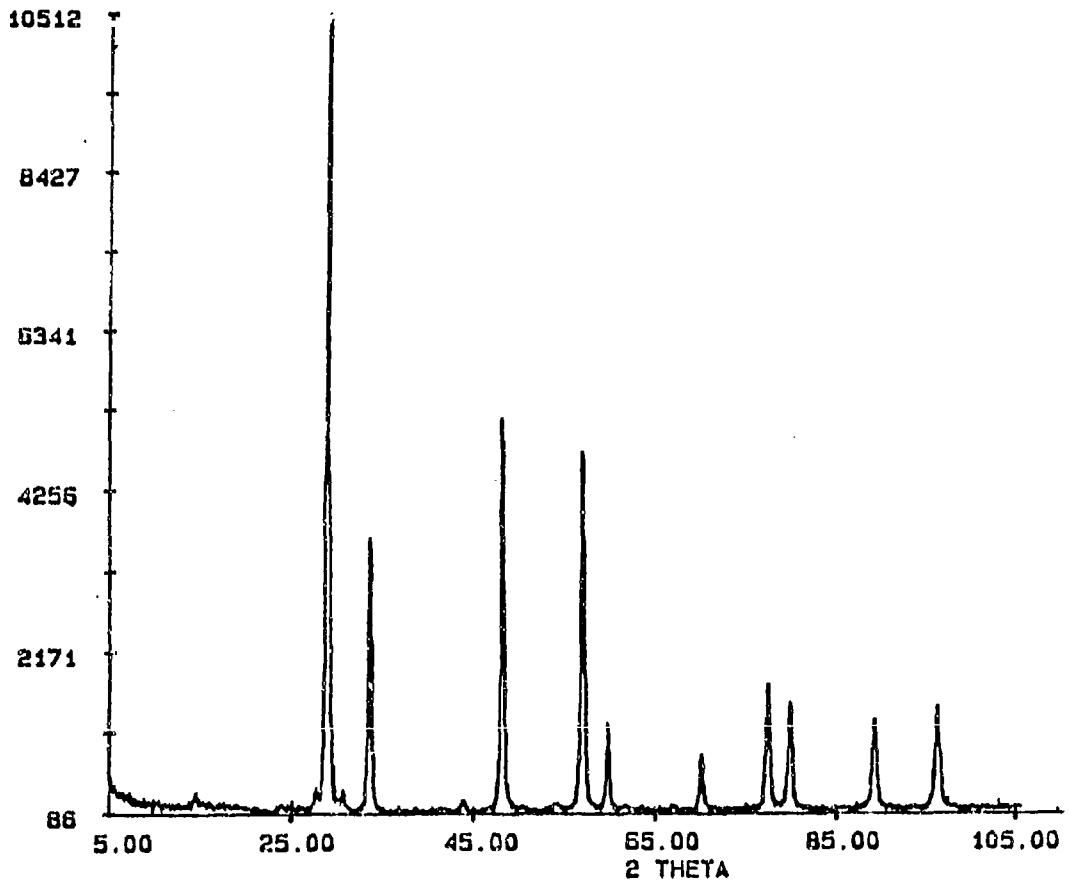

Figure 2.2 X-ray diffractometer tracing of calcined $La_2Hf_2O_7$

Table 1. X-ray Diffraction Pattern of Powder from 7a

2Θ Obs	2Θ Calc	hkl	I_{obs}/I_{100}	I_{calc}/I_{100}
29.2	29.2	111	100	100
33.6	33.2	200	34	40
48.1	47.8	220	49	65
56.9	56.7	311	45	55
59.7	59.4	222	11	16
70.2	69.8	400	7	10
77.5	77.2	331	16	25
79.9	79.6	420	14	22
89.3	89.0	511/311	12	18

No extraneous lines were observed in the spectrum and differences between standard and observed line intensities are attributed to preferred orientation. The fact that lanthanum hafnate was the only phase present indicates that 1100°C is an adequate temperature to fully react the co-precipitated oxides.

The product in 7b. was an amorphous stoichiometric mixture of $2HfO_2$-La_2O_3 and did not yield a suitable x-ray pattern.

Material from 7a. was strongly sintered and very hard to grind. A small amount of ground sinter, the bulk of which was extremely fine (<37 um), was prepared for plasma spray coating studies.

By contrast, the product obtained in 7b. was an agglomerate of micron sized particles that was easily comminuted into different size fractions. Because of the ease in preparing powder feed from this source, it was decided to study conditions to produce lanthanum hafnate <u>in situ</u> during plasma spraying of the unreacted co-precipitated powders.

2.2 Plasma Spraying of Lanthanum Hafnate

2.2.1 Coating Methodology

Lanthanum hafnate melts congruently and, therefore, can be plasma sprayed without composition change. The parameters used during plasma spraying greatly affect the microstructure of the deposit. Coatings can be prepared which are either highly dense or have significant microporosity built into their structure. Although microporosity can subject the substrate to somewhat higher fluxes of oxygen, the more open structure will aid in relieving stresses which occur during thermal cycling. In the case where an inert iridium diffusion barrier layer acts as a total diffusion block, an outer coating of lanthanum hafnate with controlled porosity may prove superior to a monolithic outer coating.

Some sintering of porous coatings may occur during coating exposure to temperatures in the 1600 - 2000°C range. Based on our studies of sintering of lanthanum hafnate coupons, prolonged exposure at the higher end of the temperature range would be required to significantly reduce coating porosity.

A series of hafnate coatings were plasma sprayed on alumina substrates in order to investigate 1) the ability to use the mixed oxide powder product obtained in 7b. to produce lanthanum hafnate coatings, and 2) methods of varying the microporosity during plasma spraying.

Alumina substrates were chosen for the initial plasma spray studies. They were degreased in 1,1,1 trichloroethylene and then rinsed in methyl ethyl ketone. The substrates were then mounted

in the fixture depicted in Figure 2.3 and grit blasted with 20 gamma alumina-3% titania grit at 65 psi with the nozzle 3 inches from, and perpendicular to them. Substrates were removed from the fixture, subjected to a jet of 100 psi clean, compressed air, and degreased. Substrate surfaces were uniformly cratered.

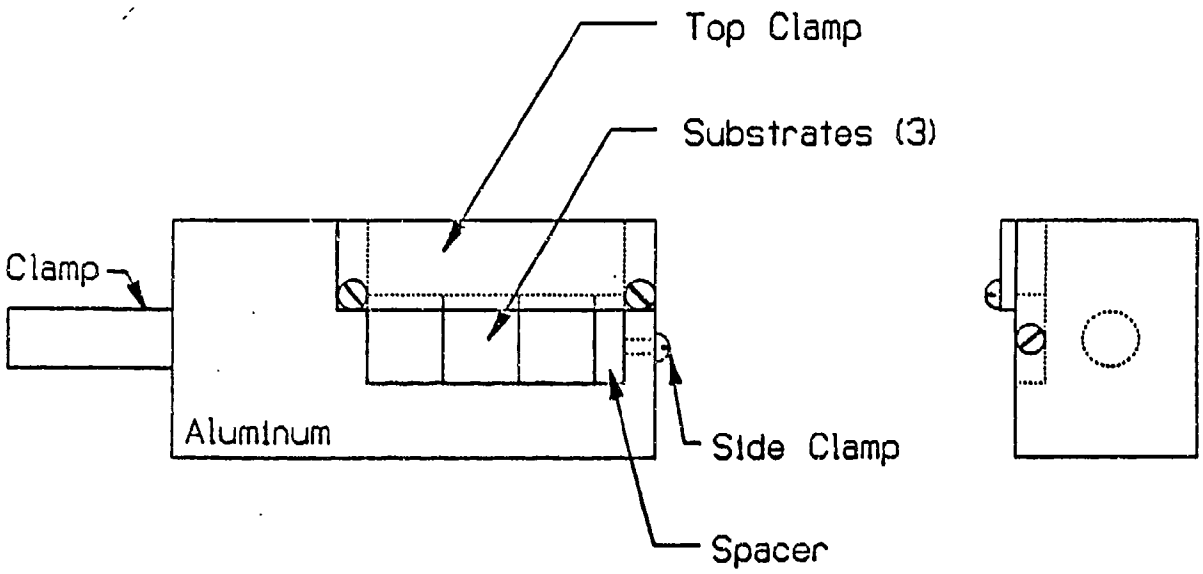

Figure 2.3. Schematic Diagram of Fixture to Hold Substrates for Plasma Spraying and Grit Blasting.

The substrates were again mounted in the fixture, three at a time, and the fixture was clamped in the spray booth. Spray coating was performed by Avalon Materials Technology (Harvard, MA) using a Perkin Elmer-Metco MN plasma system rated at 40KW and fitted with a 3MB hand-held gun. The powder was fed to the gun with a Metco 4MP fluidized bed powder feeder set for spraying fine ceramic powders.

The plasma spray gun was ignited and first used to preheat the substrates to 200°C to remove adsorbed contaminants. Surface temperatures were measured using a Type K thermocouple with digital readout. The coatings were applied by traversing hori-

zontally across the substrates at approximately 1 meter/sec and indexing down approximately 1 cm per pass. Nominal spray conditions are shown in Table 2.

Table 2
Parameters used in plasma spraying lanthanum hafnate.

a. argon 80 SCFH, hydrogen 17 SCFH
b. 70V dc, 500A DC
c. powder carrier gas: argon at 37 SCFM
d. powder feed rate: 90
e. powder port shaft: B
f. powder port: 2
g. feed hose: black
h. vibrator pressure: 20 psi
i. spray distance: 75 mm
j. siphon air: none

2.2.2 Plasma Spray Results

The very fine powder obtained by grinding the sinter (Section 2.1, step 7a.) was difficult to spay and resulted in very low coating efficiency. A fracture surface of a 35 um coating is shown in Figure 2.4. The coating was tightly adherent and exhibited very low porosity.

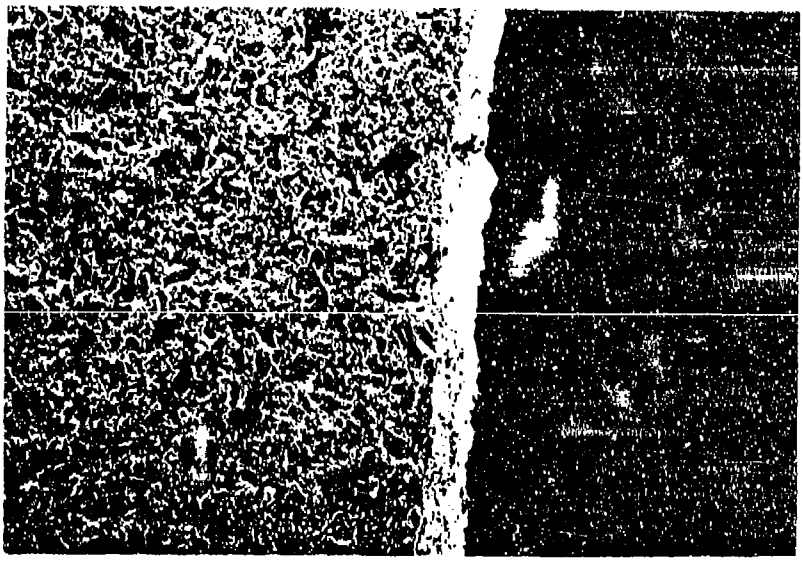

Figure 2.4 Cross-section of plasma sprayed $La_2Hf_2O_7$ on Al_2O_3. 200X

The powder agglomerate described in Section 2.2, step 7b. was sieved to several size fractions. Attempts to plasma spray coatings using the coarse powder fraction (74 - 125 um) were unsuccessful. Melting was incomplete and the powder did not adequately adhere to the substrate

The medium powder size fraction (37 - 74 um) performed well during spraying. Very little fuming was observed, indicating that the plasma was not too hot, the deposition efficiency was acceptable, and much of the powder was melted during the spraying.

Coated samples were cut in half and one-half of each was heat treated in air at 1650°C. Most samples were cross-sectioned, polished and examined. Some samples were simply fractured before SEM examination.

A fracture cross-section of a 70 um thick coating prior to heat treatment is shown in Figure 2.5. The microstructure shows the typical laminar structure of a plasma sprayed coating parallel to the substrate that results from scanning the plasma gun to build up coating thickness. Figure 2.6 shows a polished cross section of the same sample which has a porosity of 5 to 10%. Figure 2.7 shows the surface of a plasma sprayed coating exhibiting areas of melted material interspersed with some smaller - possibly unmelted - particles.

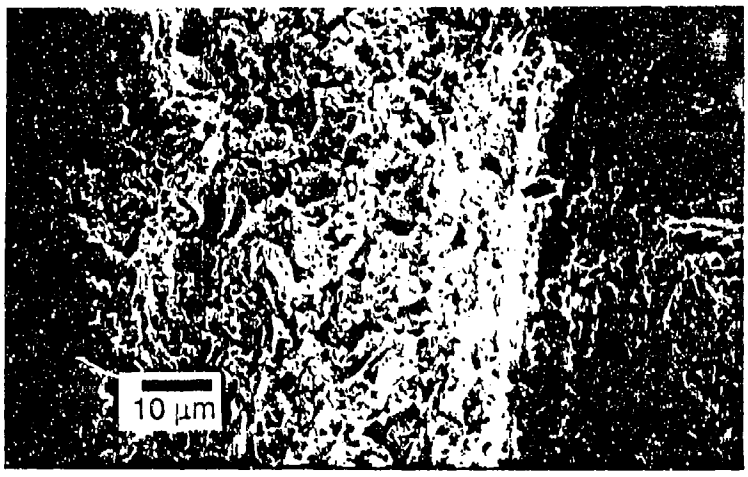

Figure 2.5 Fracture cross section of a plasma sprayed lanthanum hafnate coating on an alumina substrate.

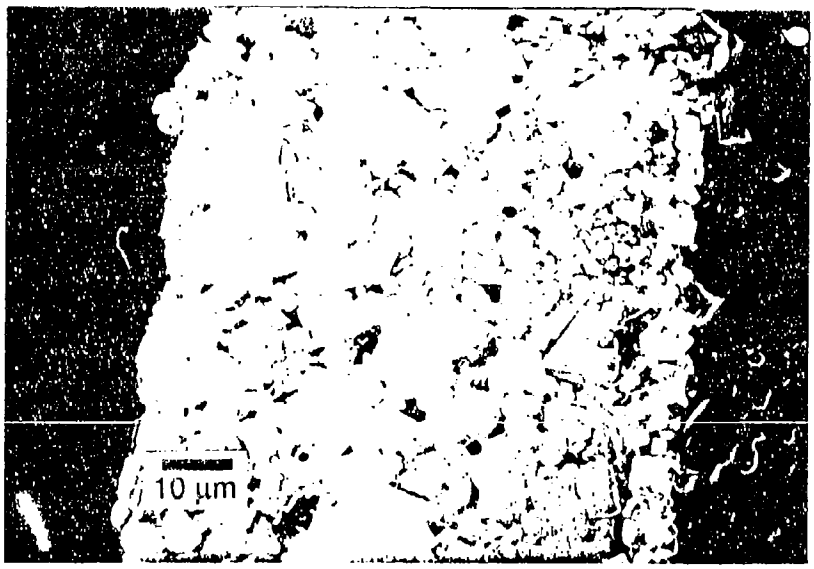

Figure 2.6 Polished cross-section of a plasma sprayed lanthanum hafnate coating on an alumina substrate.

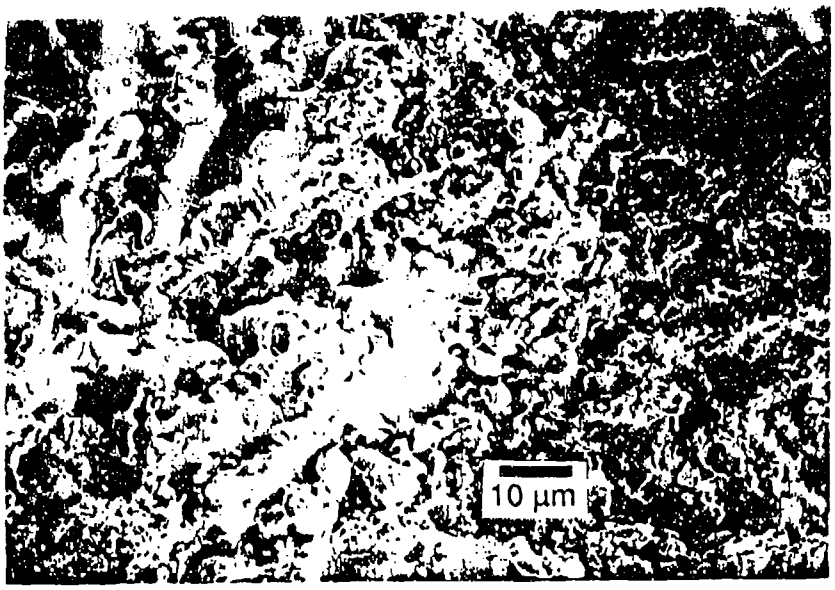

Figure 2.7 Surface of plasma sprayed lanthanum hafnate coating.

Coating adhesion was measured by a pull test on a stud epoxied to the coating surface (ASTM D 4641). A pull-off strength of 3000 PSI was measured for the best coatings in the as-deposited condition on alumina. Adhesion was also measured after heat treatment and the pull-off strength increased to over 25,000 PSI. However, metallurgical cross sections revealed that the alumina had reacted with the lanthanum hafnate at the interface to produce a mixed oxide diffusion zone which probably enhanced the adherence.

The extent to which the lanthanum hafnate pyrochlore structure forms from the mixed oxide powder feed during the brief period of plasma spaying was established by x-ray diffraction (XRD). Plasma sprayed coatings were examined both before and after heat treating to 1650°C and XRD scans are shown in Figure 2.8. Table 3 shows the d-spacings and calculated two-theta

values for hafnium oxide, lanthanum oxide and lanthanum hafnate for copper K-alpha radiation (1.542Å).

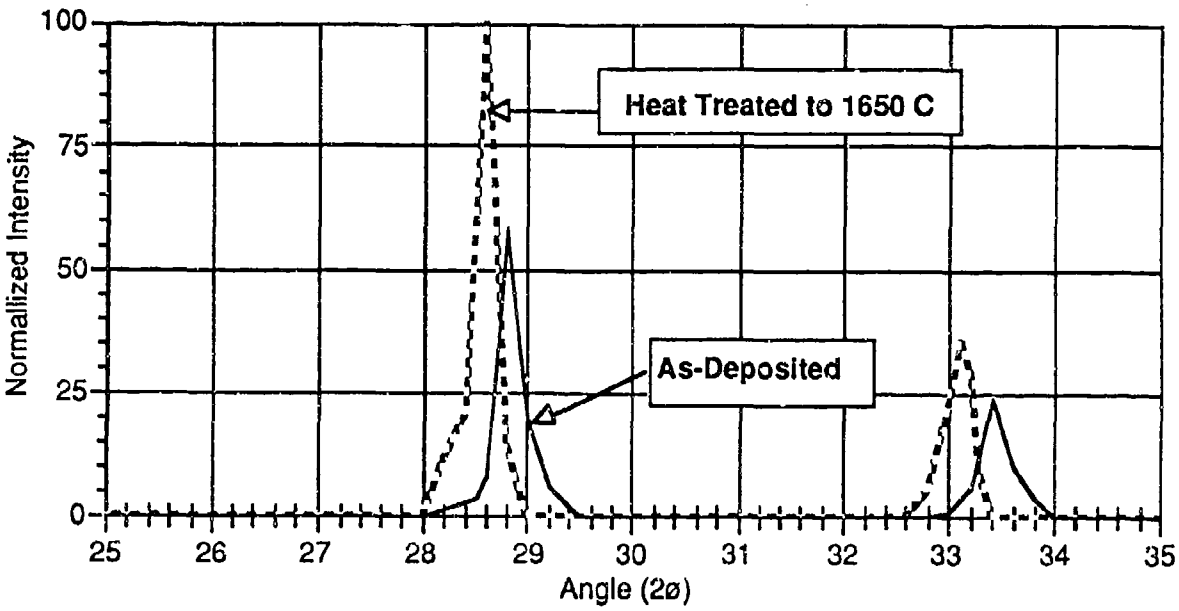

Figure 2.8 X-ray diffraction pattern of plasma sprayed lanthanum hafnate coating before and after annealing at 1650°C.

Table 3
Literature values for d-spacings and intensity of hafnia, lanthana and lanthanum hafnate

Compound	d (Å)	2θ	I/I°
HfO_2	3.15	28.34	100
	2.82	31.73	100
	2.59	34.64	60
	5.07	17.49	20
La_2O_3	3.27	27.27	100
	2.00	45.34	40
	2.83	31.61	35
	4.62	19.21	10
$La_2Hf_2O_7$	3.11	28.68	100
	2.69	33.24	40
	1.90	47.83	65
	1.62	56.78	55

There is an excellent match of both peak position and intensity for the heat treated coating with the published values for lanthanum hafnate. (The 65% intensity peak at a two-theta of 47.8^{o} was also observed at the proper location but is not shown in Figure 2.8.) The as-deposited coating also exhibits the lanthanum hafnate structure, except that the peaks are less sharp and there is a small shift to higher two-theta angles. The shift can likely be attributed to the very rapid cooling of the plasma sprayed material which results in lattice strain.

2.3 Plasma Coating Lanthanum Hafnate on Iridium

In the duplex coating under development lanthanum hafnate is the outer layer over the **CAFRIB** configuration. To determine the feasibility of coating lanthanum hafnate on iridium, a C-C sample coated with 5 um of iridium deposited from the molten salt electroplating bath was plasma sprayed with a 70 um layer of lanthanum hafnate. A photomicrograph is shown in Figure 2.9. The lanthanum hafnate layer was well-bonded to the iridium.

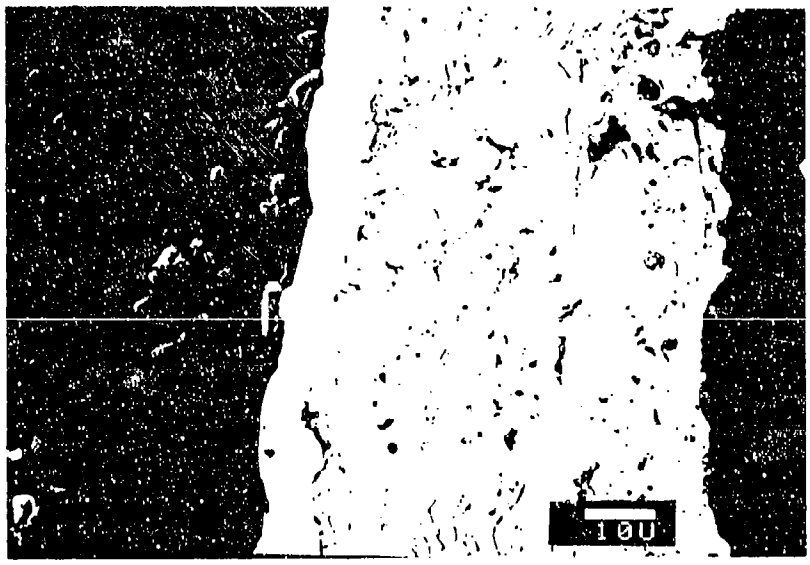

Figure 2.9 Cross-section of an iridium/lanthanum hafnate duplex layer coating on a carbon-carbon composite.

3. CAFRIB INNER BARRIER LAYER

3.1 Carbon-Carbon Composite Material

Two-dimensional carbon-carbon composite was obtained in the form of 3 mm thick sheets from Carbon Carbon Advanced Technologies (C-CAT) of Fort Worth, TX. The reinforcing material was Amoco T-300 woven graphite fibers with a density of 1.76 g/cm^3. Woven fibers occupied about 55 volume percent of the composite. The char matrix, whose density was about 1.8 g/cm^3, occupied 35 volume percent of the composite and 7 volume percent was void space. Samples were cut with a fine blade saw to dimensions of 1 cm x 1 cm x 0.3 cm. Cross-sections showed that portions of the surface of the C-C were covered with a residual layer of about 5 um of char.

3.2 Preparation of Matrix-Free Zone

In order to form the **CAFRIB** barrier layer, it is first necessary to prepare a matrix-free surface zone on the C-C. The pyrolyzed carbon which makes up the matrix char is likely to be more reactive to oxidizing agents than the graphite fibers. It is, then, reasonable to assume that matrix can be selectively removed from around fibers by oxidation reactions.

The oxidation must be highly selective so that, while matrix is being removed, the graphite fibers remain virtually unattacked. This will ensure that the reinforcing property of the fibers are not undermined. Crocker and McEnaney (14) studied failure of 2-D C-C which had been oxidized at 700°C and found a decrease with weight loss of flexural strength and elastic modulus. At 2% weight loss the flexural strength decreased by 9% and the elastic modulus by 5%; at 6% weight loss the flexural

strength decreased by 21% and the elastic modulus by 11%. These mechanical property degradations are more extreme than we believed was necessary since, at 700°C, we observe both fiber and matrix attack.

In this study three methods were examined to effect selective matrix removal: reactive ion beam etching, anodic oxidation and thermal oxidation.

3.2.1 Reactive Ion Etching

Reactive ion etching (RIE) uses a plasma to remove material from a surface through a synergistic combination of sputtering and chemical reaction. The sample to be etched is charged with DC or radio frequency in a vacuum chamber to form a plasma of energetic electrons, ions and neutral species. Surface carbon is removed by reaction to form CO and CO_2. The typical process parameters used in this study are listed in Table 4.

TABLE 4
Conditions for Reactive Ion Etching of C-C

RF Frequency	13.56 MHz
RF Power	2-5 watts/cm^2
Pressure	10 mtorr
Gas Mixture	50-50 Argon-Oxygen
Temperature	less than 100°C
Time	15 minutes

A photomicrograph of the surface of 2D C-C after REI is shown in Figure 3.1. The bottom part of the sample was masked during exposure. Two exposure times were used with the upper region of the sample having the longer time. Only moderate selectivity was observed between surface and fiber removal. Only surface matrix was removed and microtexturing of the entire surface, including fiber attack, was observed.

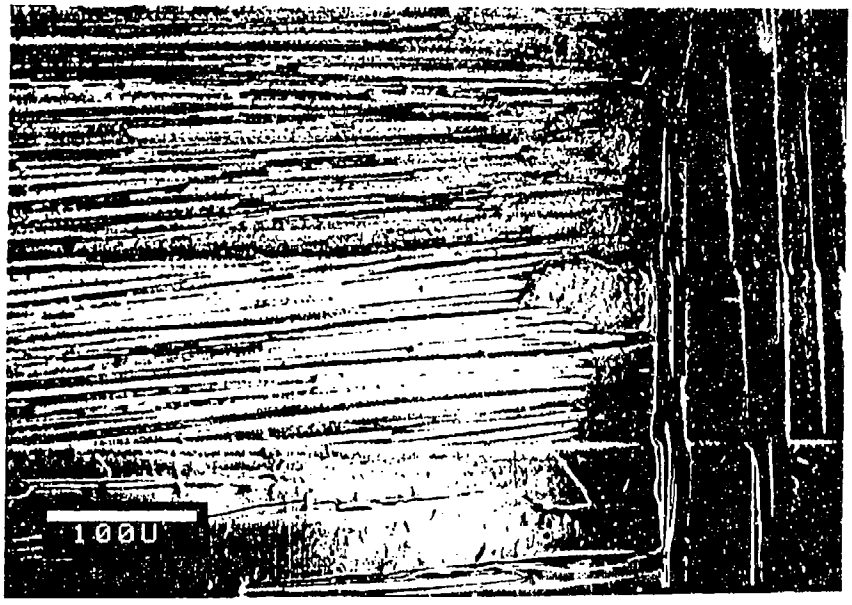

Figure 3.1 Reactive ion etching of 2D carbon-carbon surface.

3.2.2 Anodic Oxidation

Anodic oxidation studies were carried out in 5-20 w/o sulfuric acid solutions using current densities from 25-250 ma/cm^2 and temperatures of 25-75°C. Some increase in reactivity was observed at higher acid concentrations and temperatures but current density was the most significant variable affecting anodic oxidation. Figure 3.2 shows the approximate depth of removal of matrix as a function of current density in 10 w/o sulfuric acid at 50^{oC}. Although matrix is adequately removed, attack also occurs on fibers and the fiber thickness is reduced near to the solution interface.

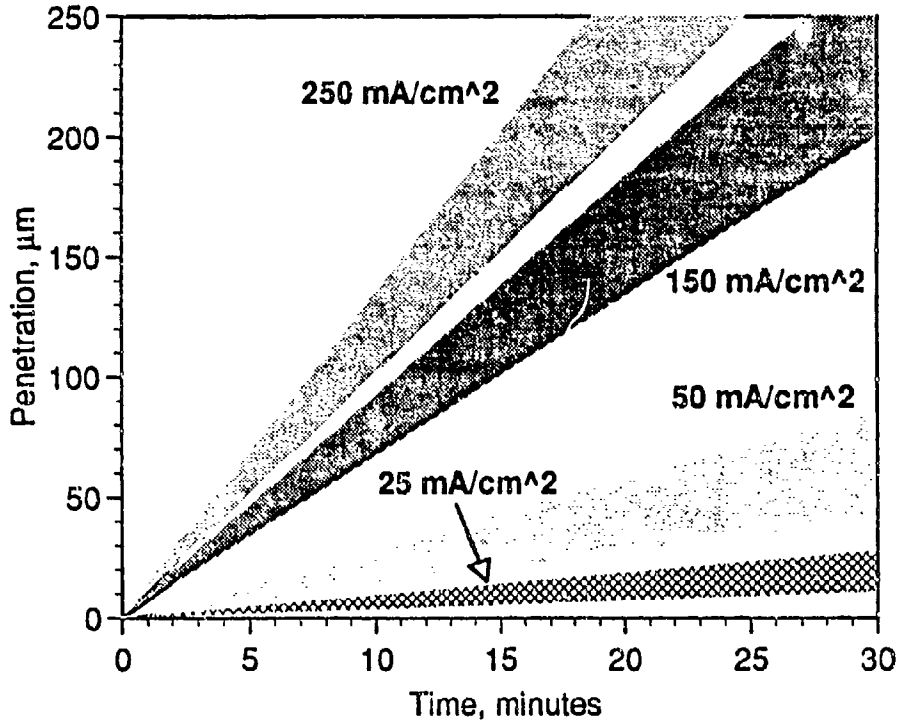

Figure 3.2 Char removal depth during anodic oxidation of C-C in 10w/o sulfuric acid at various current densities.

It may be possible to find other electrolytes or conditions which will be more selective for char removal but, since thermal oxidation proved a superior method, the anodic oxidation route was abandoned.

3.2.3 Thermal Oxidation

Thermogravimetric analysis (TGA) studies of C-C and bundles of carbon fibers demonstrated the marked difference in the oxidation rate of fiber compared with matrix. Preliminary isothermal oxidation studies on composite at a temperature of 550°C showed that matrix oxidation proceeds from the C-C surface inward with no visible attack on fibers even after matrix removal to a depth

of 20 fiber diameters, i.e., 120 um. The surface of a sample before and after oxidation is shown in Figure 3.3. The intact fibers after oxidation are seen in relief.

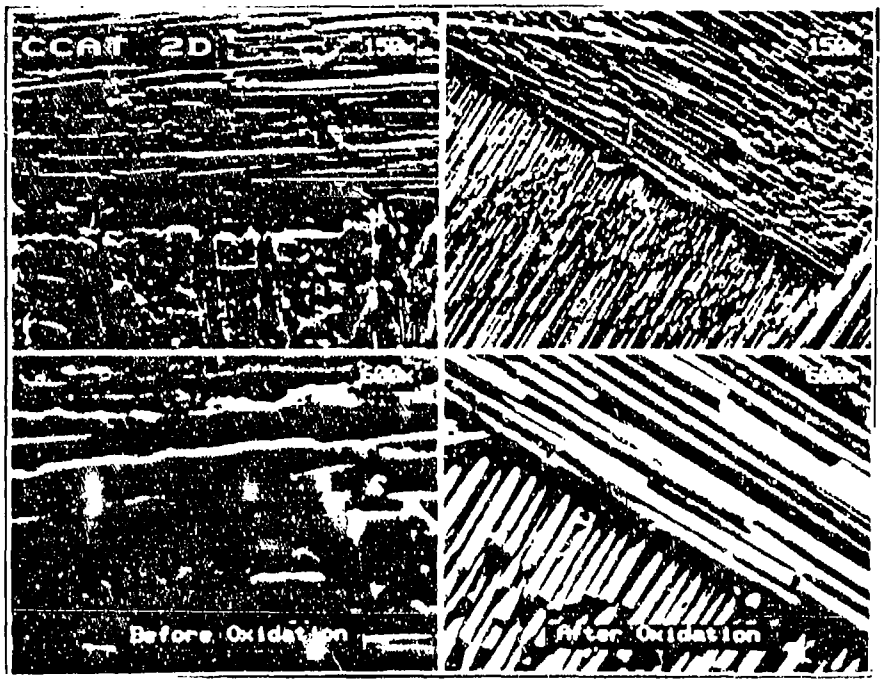

Figure 3.3 Surface view of 2D carbon-carbon before and after selective oxidation to remove surface char. Actual magnifications are one-fourth of those shown.

The outermost surface layer of char (see Section 3.1) appeared to be more refractory than the char within the composite and retarded surface oxidation where it was present. It may be that the outer char becomes partly graphitized during final resin curing. In any case, it was considered expedient to sand the outer surfaces to remove the char layer prior to oxidation.

A polyvariable statistical experimental design was used to measure C-C oxidation rates and establish parameters for preparing surface zones free of char. Samples were exposed in air in a laboratory furnace for periods of 10 to 70 minutes at temper-

atures between 500 and 550°C. Figure 3.4 shows contour weight loss plots as a function of time and temperature.

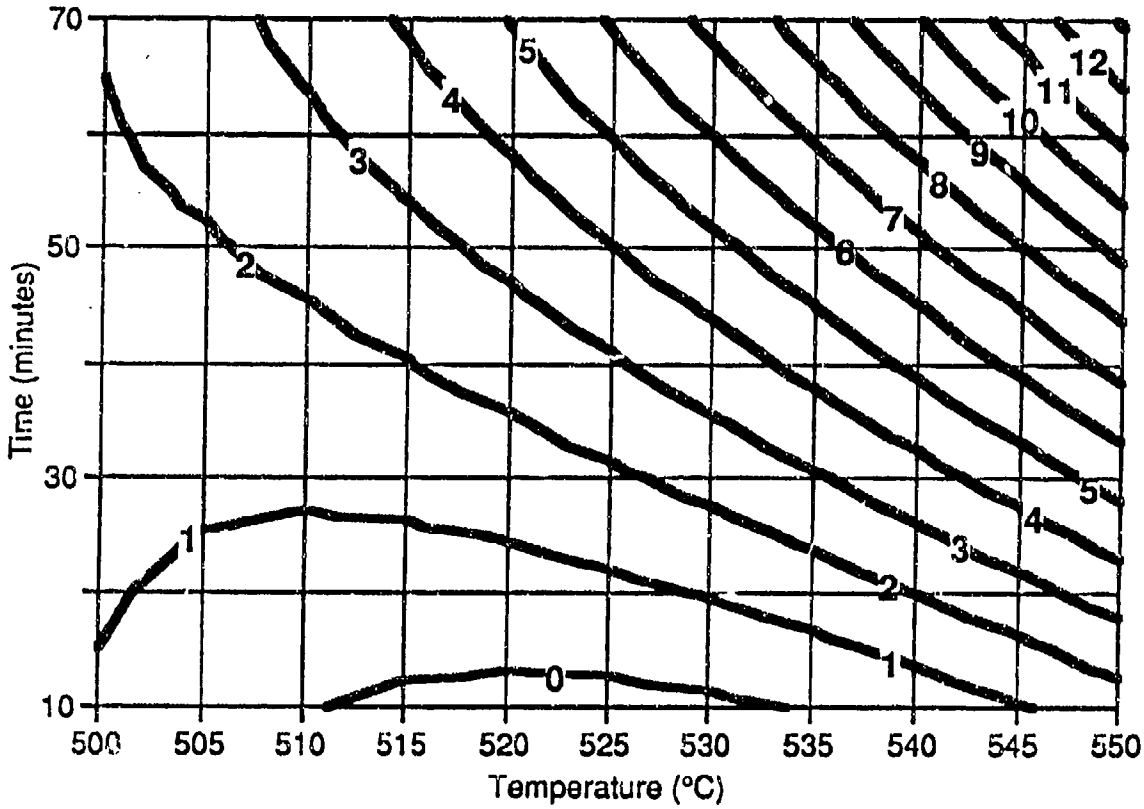

Figure 3.4 Contour plot of the oxidation weight loss of carbon-carbon as a function of time and temperature.

Oxidized C-C coupons were split open and epoxy resin impregnated under vacuum to fill void spaces. Samples were then mounted, polished and examined microscopically in cross-section. It was sometimes difficult to obtain good contrast between the mounting material and remaining char so that depths of char removal were hard to assess. Electrodeposition of nickel into the sample surface prior to resin impregnation enabled us to obtain good contrast between void and remaining char. This also ensured that the void depth measured was accessible to electro-

chemical metal impregnation so that the **CAFRIB** layer could be formed to that depth.

Figure 3.5 shows the surface of a C-C composite oxidized for 530°C for 1 hour and impregnated with nickel. The depth of nickel penetration ranged from about 4 to 7 fiber diameters, or 24 to 42 um, with an average depth of 30 um. Penetration tends to be greater on the edges of a sample where fiber cross sections intersect the edge. It may be that oxygen is able to penetrate more readily longitudinally along fiber/char interfaces. On the sample surface, areas where fibers cross at the weave tend to oxidize more slowly, probably as a result of restricted oxygen access to these areas.

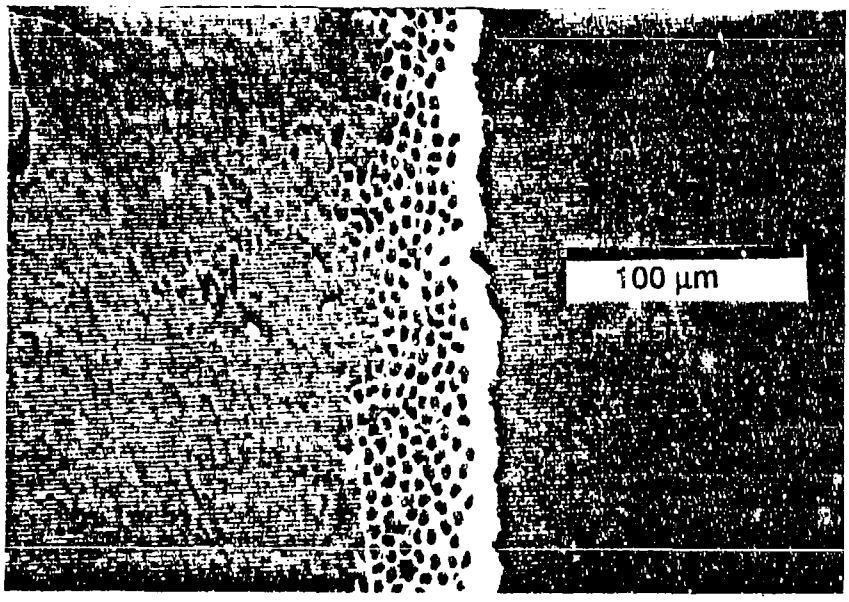

Figure 3.5 **CAFRIB** layer infiltrated with nickel.

Samples oxidized at various times and temperatures were infiltrated with nickel and the average depth of char removal was measured. These data are presented in Figure 3.6.

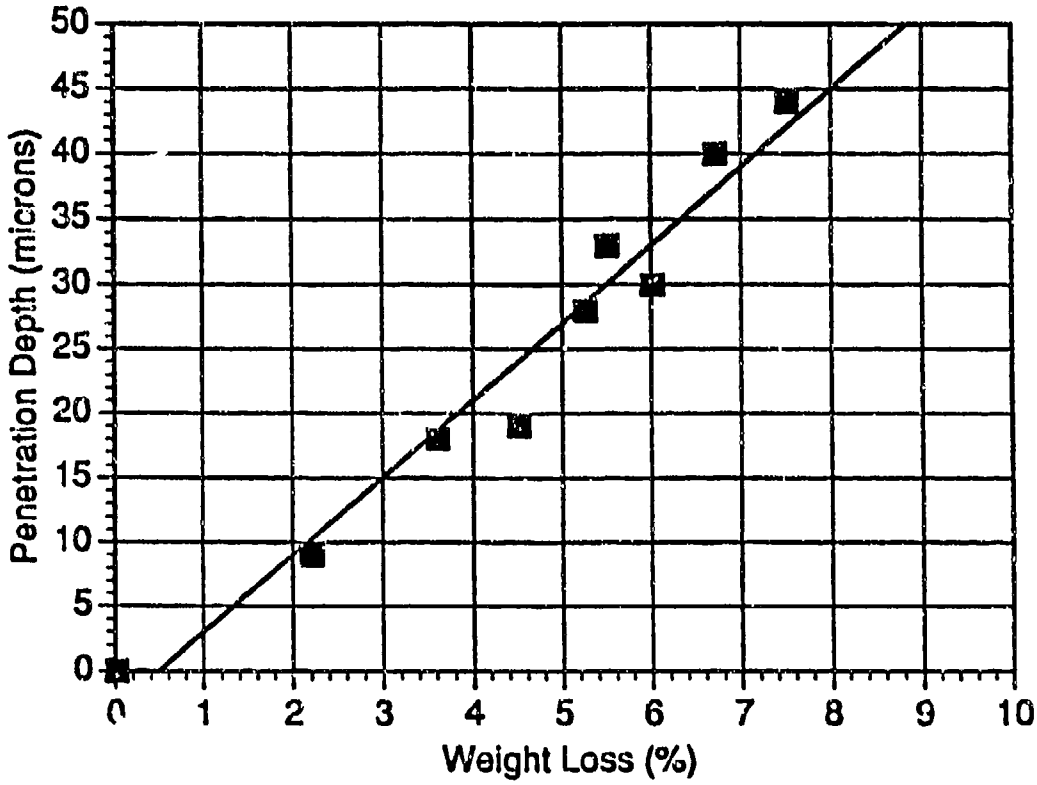

Figure 3.6 Depth of the char-depleted zone as a function of weight loss.

Comparison of Figures 3.4 and 3.6 enabled us to establish the relation between weight loss and penetration depth. For example, the sample shown in Figure 3.5, which showed an average penetration depth of 30 um, had a weight loss of about 6 w/o. A contour plot of depth of matrix char removal as a function of time and temperature is shown in Figure 3.7.

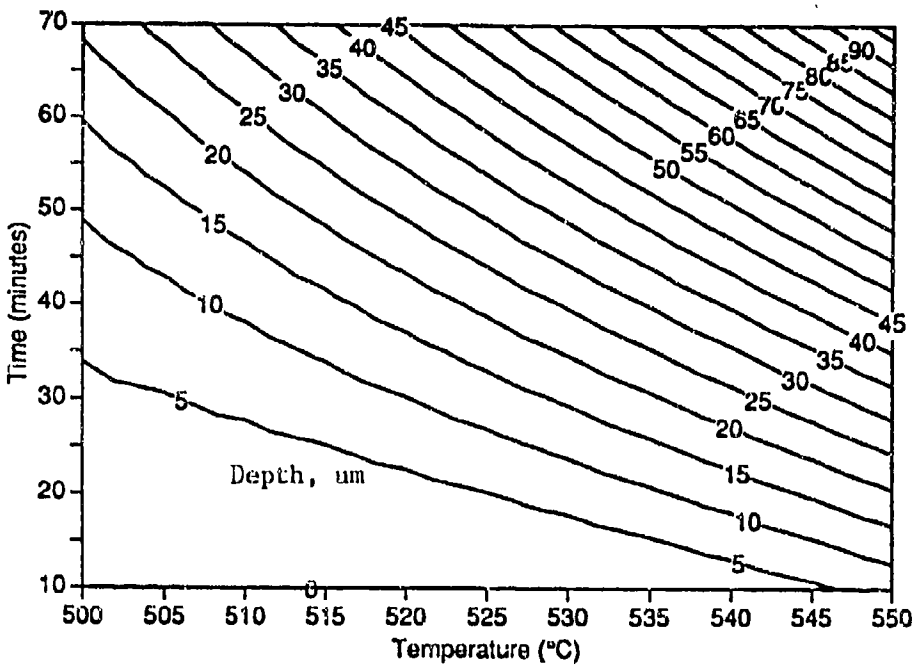

Figure 3.7 Depth of matrix char removal as a function of time and temperature during oxidation in air.

The theoretical weight loss for the removal of char to a specific depth can be calculated from the fiber and char densities and volume fractions given in Section 3.1. The theoretical weight loss for a 30 um char-depleted zone is about 3 w/o. Since the observed weight loss for 30 um depletion is 6 w/o, about half of the weight loss is attributed to char oxidation below the depleted zone. This could lead to some weakening of the composite below the **CAFRIB** layer.

In order to devise a better oxidation protocol which did not weaken the substrate, oxidation studies were performed at various oxygen pressures and temperatures. Oxidation at reduced pressure was found to be more selective for surface char removal without substrate attack. A plot of weight loss vs. char depletion during oxidation in 5 volume percent oxygen at 590°C is shown in Figure 3.8. Oxidation at 590°C for 35 minutes gives a 30 um

char-depleted zone at a weight loss of only 3 w/o which is, within experimental error, identical to the theoretical value. The low oxygen pressure protocol was, therefore, adopted for preparing substrates for the **CAFRIB** layer.

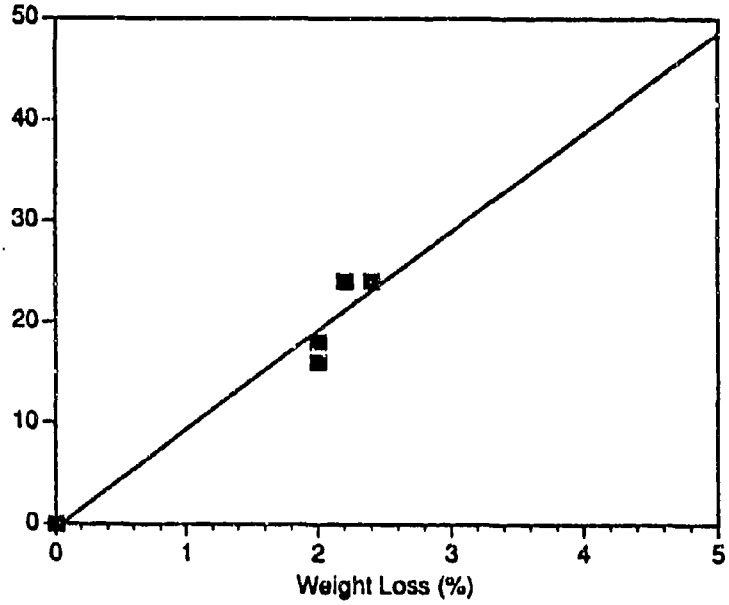

Figure 3.8 Matrix char removal as a function of weight loss for oxidation in 5 volume percent oxygen at 590°C.

3.3 Electrochemical Impregnation

3.3.1 Previous Studies

In a previous study (2) Castle Technology demonstrated that well-bonded iridium coatings could be electrodeposited onto graphite from a molten salt bath. During the Phase I ONR program (N00014-91-C-0119) iridium deposition studies were extended to include oxidized 2-D C-C composites. Figure 3.9 shows that penetration of iridium into oxidized C-C occurred to a depth of only one or two fiber diameters. Coverage was non-uniform and the surface was highly dendritic in some areas. During this study efforts were made to increase iridium penetration and

obtain a more uniform, less dendritic deposit.

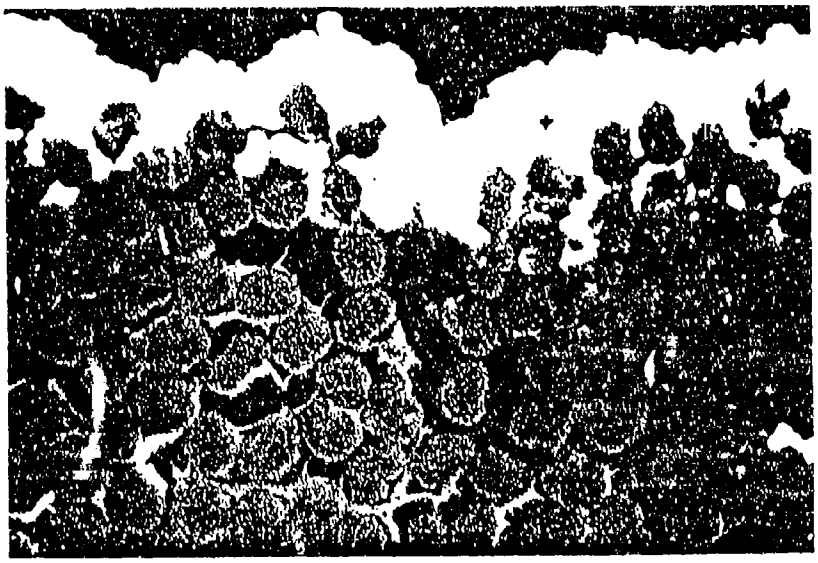

Figure 3.9 Electrodeposited iridium on oxidized carbon-carbon.

3.3.2 Molten Salt Electrodeposition of Iridium

A schematic diagram of the apparatus used in the electrodeposition of iridium from a molten salt is shown in Figure 3.10. A 15 cm diameter quartz flask with a flange seal was mated to an upper Pyrex section fitted with five ground glass ta[illegible]ints. Electrodes entered the flask through two side joints [illegible]stirrer, gas sparge line, and thermocouple well (not sho[illegible]er through large center joints. The electrolytic cell w[illegible]ted by a resistance furnace. 6M NaOH solution was used to scru[illegible]lorine gas from the system prior to venting.

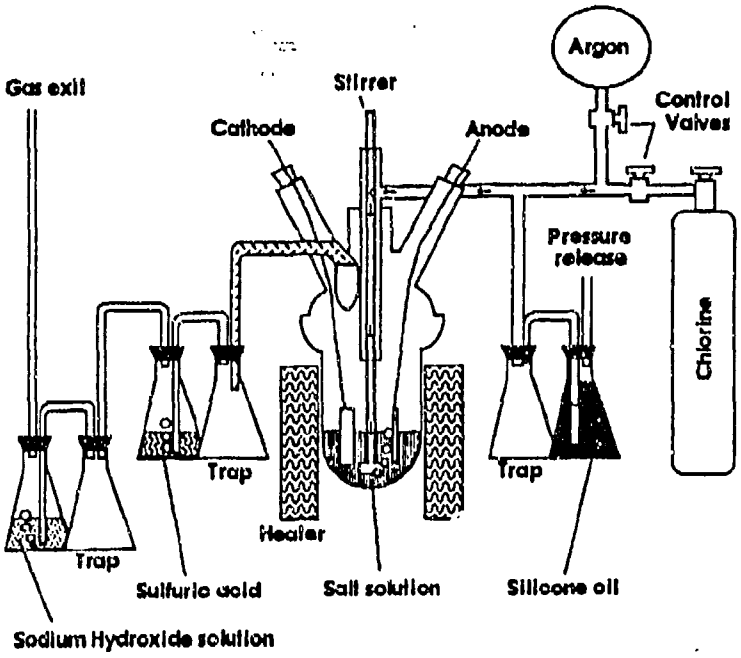

Figure 3.10. Schematic diagram of apparatus for Iridium Plating.

The molten salt composition is that reported by Saltykova et. al. (17) and consists of NaCl, KCl, CsCl and $IrCl_3$ in the molar ratio 30: 24.5: 45: 0.5. The mixture is extremely hygroscopic and oxide hydrolysis products are known to have deleterious effects on iridium deposition. Prior to electrodeposition, the melt was purified by passing chlorine gas through it to remove oxides by reaction to form volatile oxy-chlorides.

Electrodeposition was performed at a temperature of 575-590°C and a current density of 10-30 mA/cm^2. A pyrolytic graphite rod was used as the anode. Iridium chloride was added to the molten salt bath as required to replenish the metal removed by plating so as to maintain an adequate iridium ion concentration.

The bulk of the studies were performed on C-C which had been

oxidized in a time-temperature regime sufficient to produce a char-depleted zone of 20-30 um.

Initial deposition studies confirmed the difficulty in filling the internal **CAFRIB** zone. During electrodeposition, there is a competition between exterior and interior fibers for metal deposition. As deposition proceeds, electrolyte in the char-depleted interior zone becomes impoverished in iridium ions more quickly than electrolyte at the exterior fiber/electrolyte interface which has ready access to fresh electrolyte. Internal deposition ceases when the surface iridium deposit bridges over and prevents access of fresh iridium-rich electrolyte to the interior fibers.

Electrolyte baths with good throwing power, such as the nickel Watts bath, are able to fill the **CAFRIB** zone with metal before bridging over (see Figure 3.5). Unfortunately, the iridium molten salt bath did not function in this manner.

Another reason that could account for the inability of iridium to fill the interior region is that electrolyte does not readily wet the carbon fibers and, therefore, does not fill the open fiber structure in the surface layer. To evaluate wetting, solidified electrolyte was placed on a C-C surface in a furnace and observed as it melted. The molten salt formed a spherical droplet on the C-C surface indicating that little wetting occurred.

In an effort to improve penetration of electrolyte into the open carbon fiber weave, the electrodeposition cell was evacuated prior to immersing the C-C cathode into the molten salt bath. This would remove air from the char-depleted zone and could allow

THIS

PAGE

IS

MISSING

IN

ORIGINAL

DOCUMENT

PAGE 35 MISSING

3.3.3 Aqueous Deposition of Iridium

No aqueous electroplating bath is commercially available for the deposition of iridium. During the 1960's several investigations were reported on plating iridium from aqueous solutions. Some success was achieved using baths based on chloride-sulfamate (16), bromide (17), and chloroiridates (18). Although deposit thicknesses of up to 25 um have been reported, deposits thicker than a few micrometers are highly stressed and cracked.

Attempts were made to improve the quality of the electroplate obtained from the bromide and sulfamate baths. Bath concentration, temperature and PCR techniques were investigated. A cross-section of an iridium deposit from an aqueous bromide bath is shown in Figure 3.12.

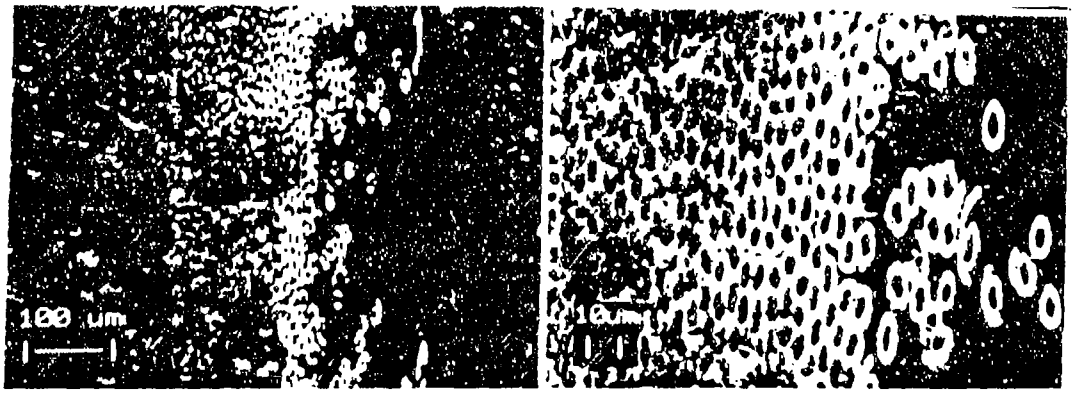

Figure 3.12 Cross-section of an iridium deposit on oxidized carbon-carbon. Note: Some fibers have broken loose and extend out from the surface.

Although penetration of iridium into the **CAFRIB** zone may be adequate, the surface of all samples were highly cracked as shown

in Figure 3.13. The high radius of curvature of the carbon fibers presents a particularly difficult substrate on which to build a strained electrodeposit as is seen in Figure 3.14.

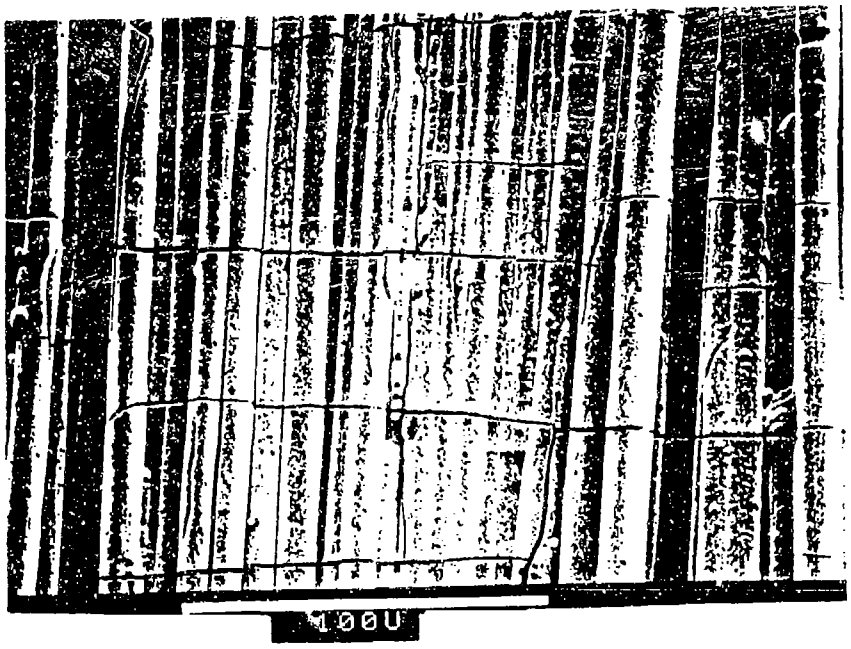

Figure 3.13 Surface of an iridium electroplate from an aqueous bromide bath.

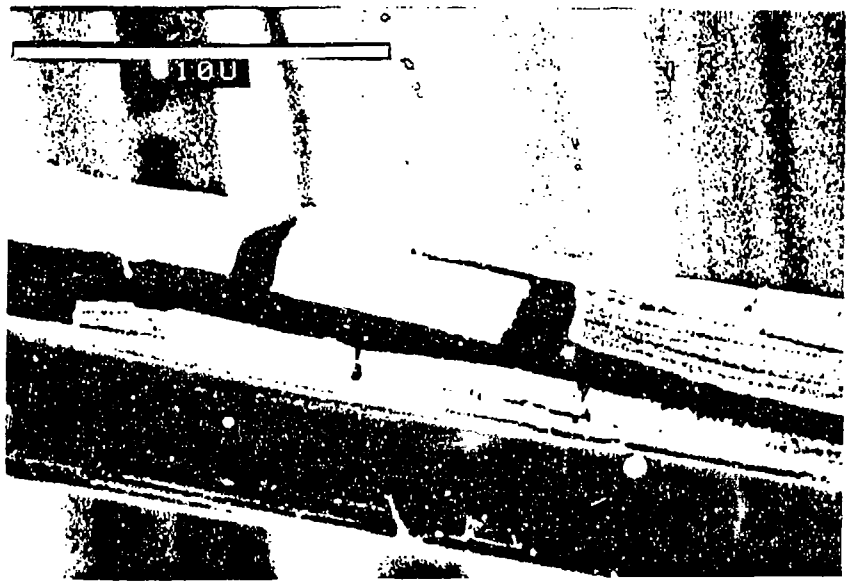

Figure 3.14 Aqueous iridium electroplate on an individual carbon fiber.

3.3.4 Aqueous Deposition of Rhodium

Commercial aqueous electroplating baths are available for the deposition of rhodium. Although the carbon-rhodium eutectic at 1694°C (19) limits the usefulness of any rhodium based coating to that temperature, the **CAFRIB** concept could be more readily investigated using rhodium electroplates. An electroplating bath based on rhodium sulfate was obtained from Technic, Inc. (Providence, RI).

Efforts to form a rhodium **CAFRIB** layer were made using samples which were oxidized to form a char-free zone of about 30 um. The results using conventional DC plating techniques are shown in Figure 3.15. Bridging over of the deposit occurred after penetration of only the topmost layer of fibers.

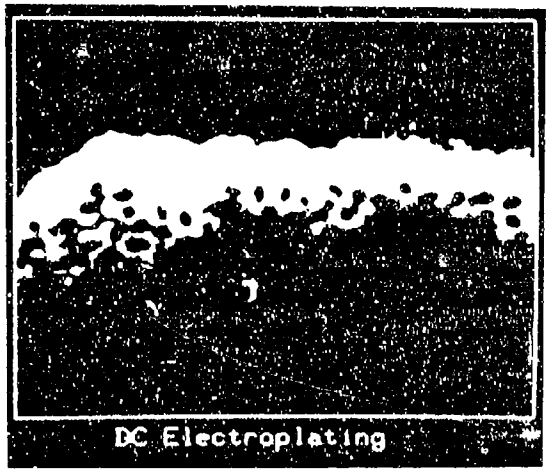

Figure 3.15 Cross-section of a DC rhodium plate from an aqueous electrolyte on oxidized carbon-carbon.

PCR techniques were then explored to improve rhodium penetration. A variety of pulse forms for both deposition and dissolution were explored. The best results were obtained using the schedule shown in Figure 3.16.

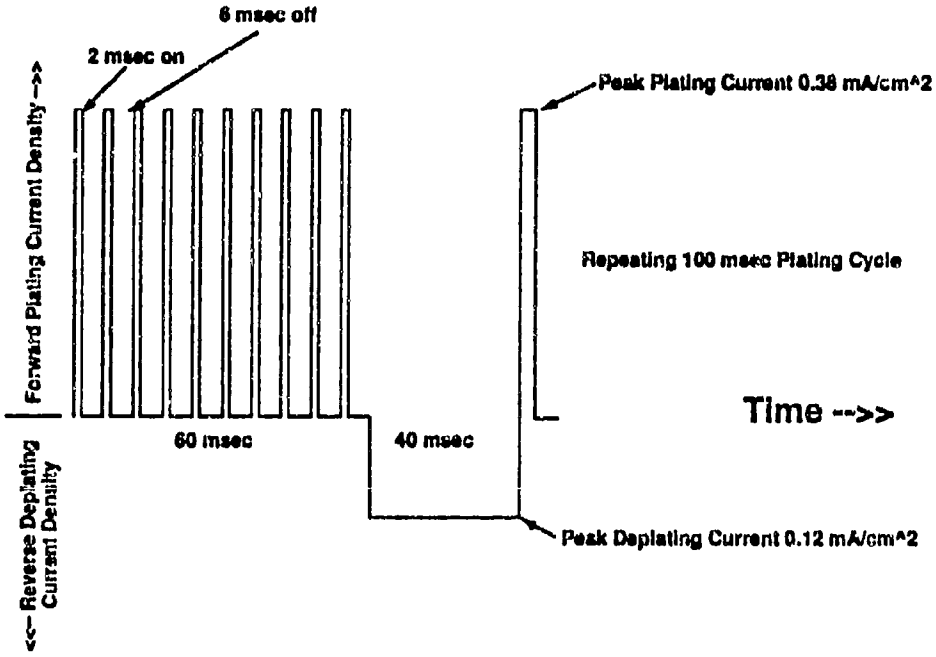

Figure 3.16 Schematic diagram of periodic current reversal protocol used in electrodepositing rhodium onto oxidized carbon-carbon.

Using this procedure we were able to fill the **CAFRIB** zone from the inside out. Figure 3.17 shows the sequence of rhodium electrodeposits as a function of deposition time.

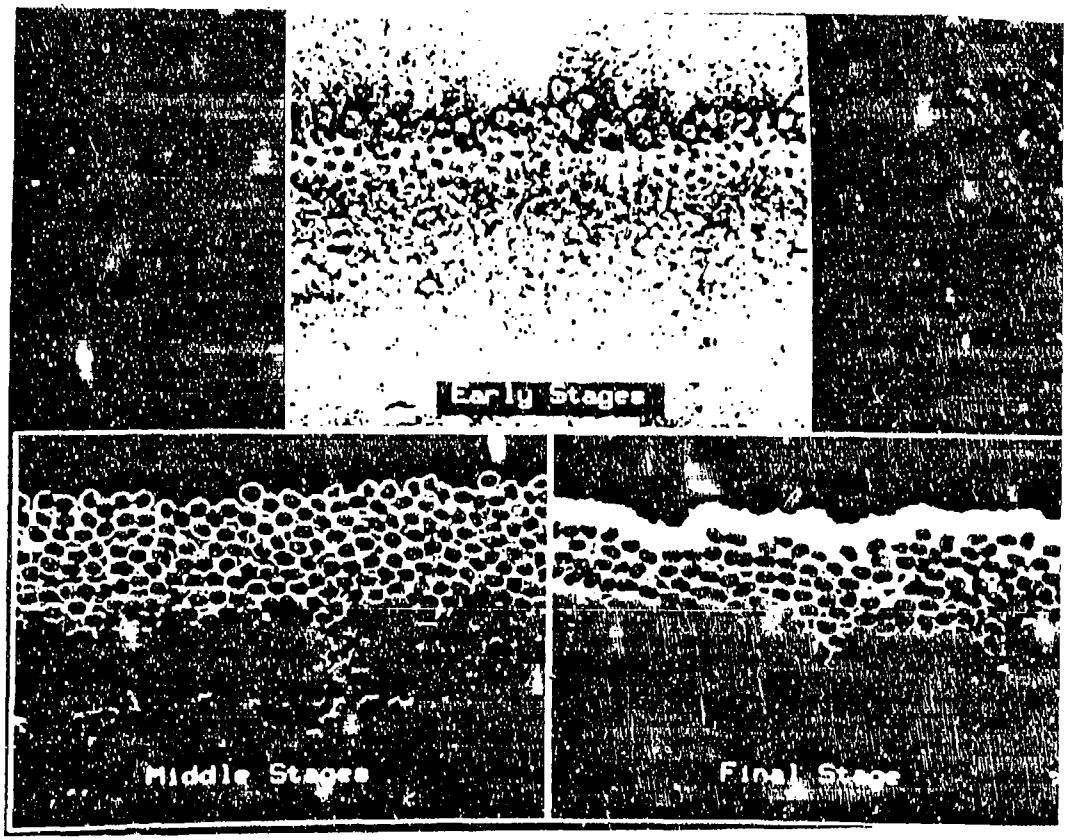

Figure 3.17 Filling of the **CAFRIB** zone in oxidized carbon-carbon composite with electrodeposited rhodium.

During the early stages only the innermost layers of the **CAFRIB** zone are filled. In the middle stages the **CAFRIB** zone is entirely filled but there is no external rhodium layer. In the final stage the **CAFRIB** zone is filled and covered with an external rhodium plate of 20 um. The ability to obtain thick coatings of rhodium on individual fibers is shown in Figure 3.18 where

6 um fibers protruding from the surface have been plated to a total thickness of about 20 um.

Figure 3.18 Rhodium electroplate on individual carbon fibers.

3.3.5 Duplex Rhodium/Iridium Barrier

The ability to infiltrate the **CAFRIB** zone with rhodium suggested that, by forming a duplex rhodium/iridium layer and diffusion annealing, the **CAFRIB** zone could be made to contain a rhodium-iridium solid solution alloy. This would raise the temperature of operation of the coating to the liquidus temperature in the iridium-rhodium-carbon ternary phase diagram at the appropriate iridium/rhodium ratio. For example, for a 50Ir-50Rh alloy, the carbon eutectic is reported to be 1932°C (19).

Samples which had been infiltrated with rhodium but had no external coating were made cathode in the iridium molten salt

plating bath and electrodeposition was attempted. Examination of these samples indicated that in many areas the infiltrated rhodium had dissolved in the molten salt bath. The external iridium layer was patchy and there were areas of uncoated C-C.

When samples which had been both infiltrated with rhodium and overplated with an external rhodium deposit of 20 um were plated, a successful iridium deposit was obtained as shown in Figure 3.19.

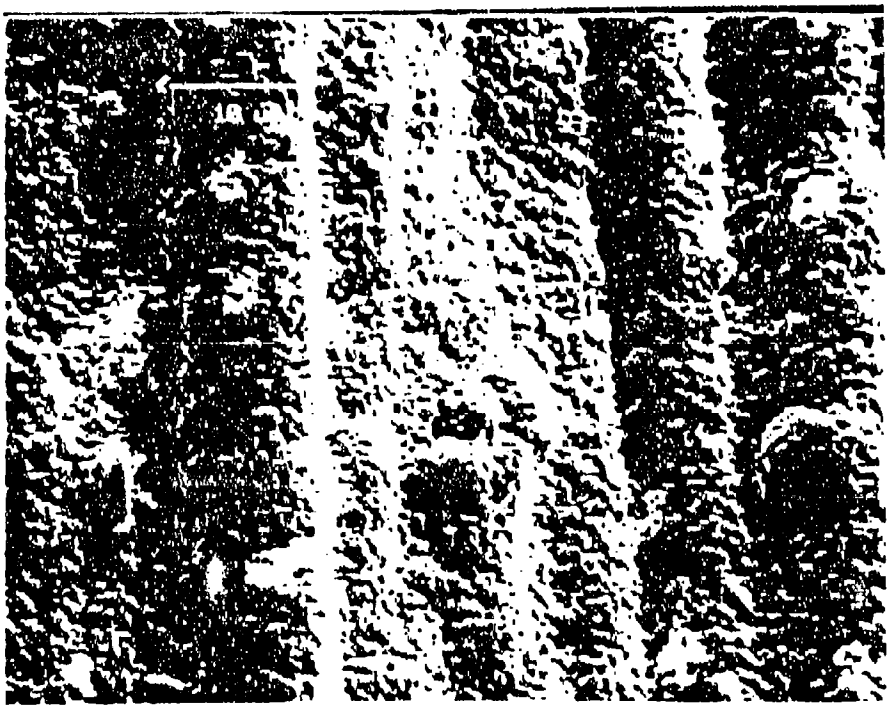

Figure 3.19 Surface of iridium deposited from molten salt onto rhodium-filled and overplated **CAFRIB**.

4. THERMAL CYCLING STUDIES

A major feature of the **CAFRIB** concept is the ability of carbon fiber reinforcements in the iridium barrier layer to absorb the stresses during thermal cycling which result from the large differences in CTE of carbon and iridium. Since we were

not successful in preparing the **CAFRIB** configuration with iridium, but were able to prepare the rhodium analog, it was prudent to attempt to test the concept with rhodium.

Samples were prepared by infiltrating rhodium to a depth of 30 um into oxidized C-C to form the **CAFRIB** configuration. Control samples were made by depositing rhodium onto C-C whose surface had been polished to remove the outer char layer. Samples were thermally cycled in an atmosphere of high purity titanium-gettered argon to 1400°C or 1600°C at a heating rate of 20°C/min and cooled at 15°C/min to 800°C after which the furnace power was turned off.

Figure 3.20 shows the surface of the control sample which had only an external rhodium deposit after cycling to 1600°C. The rhodium coating was highly cracked and in many areas the C-C substrate was visible.

Figure 3.20 Surface of rhodium plated carbon-carbon control sample thermally cycled to 1600°C.

Figure 3.21 shows the surface of C-C with a **CAFRIB** layer which has been cycled to 1600°C. Coating adherence was much superior to that observed on the control sample although cracking was observed in some areas. Small holes in the rhodium seen at high magnification may be the result of an iron impurity from the furnace which was identified in the coating by SEM.

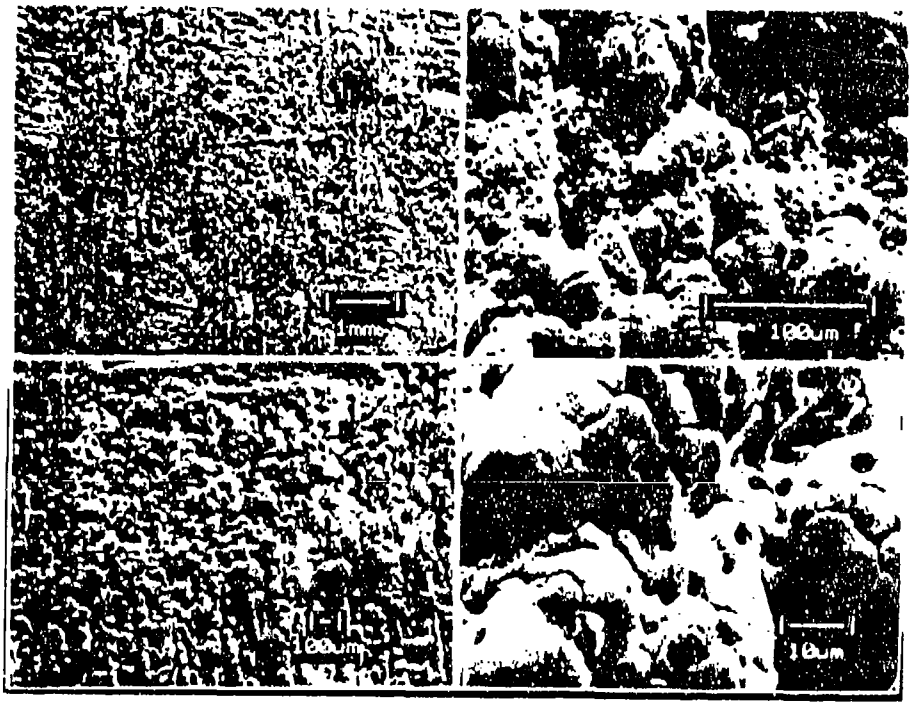

Figure 3.21 Surface of rhodium-filled **CAFRIB** thermally cycled to 1600°C.

A cross-section of a sample thermally cycled to 1400°C is shown in Figure 3.22. Much of the rhodium in the **CAFRIB** zone has pulled away from the carbon fibers and either spheridized to small rhodium globules within the **CAFRIB** zone or migrated outward to join the external coating. It is reasonable to conclude that rhodium does not wet the carbon fibers enough to prevent surface tension forces from destabilizing the carbon fiber reinforced rhodium matrix. To successfully thermal cycle a rhodium **CAFRIB**

part, it will be necessary to find a means to promote wetting of carbon fibers by rhodium.

Figure 3.22 Cross section of rhodium-filled **CAFRIB** after thermal cycling to 1400°C.

5. CONCLUSIONS

1) Lanthanum hafnate coatings of controlled porosity have been applied to iridium and rhodium by plasma spraying a co-precipitated powder mix of lanthanum and hafnium oxides.

2) Matrix char has been selectively removed by controlled oxidation from the surface of 2D carbon-carbon composites. Undamaged matrix-free woven carbon fiber surface layers have been produced to a controlled depth of 10 to 100 micrometers.

3) Iridium has been electrochemically deposited from a molten salt electrolyte onto an oxidized carbon-carbon composite but does not penetrate into the open surface layer.

4) Iridium has been electrodeposited from an aqueous electrolyte and penetrates into the open surface zone but, because of the large strain in the electrodeposit, debonds from carbon fibers and forms surface cracks.

5) Rhodium has been electrodeposited from an aqueous electrolyte using periodic current reversal techniques to successfully fill the open surface layer and form a crack-free, adherent **CAFRIB** coating.

6) Rhodium **CAFRIB** coatings which were thermally cycled to 1400°C and 1600°C exhibit greatly improved adherence and crack resistance compared with samples which were only overplated with rhodium.

7) The **CAFRIB** rhodium coating destabilizes at high temperature due to the non-wetting of carbon fibers by rhodium. Globules of rhodium form within the zone and some rhodium migrates to the outer layer.

6. REFERENCES

1. R. Boisvert and J. Diefendorf in "Proceedings of the Ultra-High Temperature Composite Materials Workshop", R. J. Kerans and L. S. Thiebert, eds., AFWAL-TR-87-4142, 1987.

2. J. P. Pemsler, "Coatings for Carbon-Carbon Composites for use at 3000°-4000°F", Final Report to AFWAL on Contract No. F33615-86-C-5094.

3. J. P. Pemsler, "Rare Earth Hafnates as Coatings for Compo- at Temperatures up to 2000°C", Extended Abstract of Electrochemical Society Meeting, Hollywood, FL, October 15-20, 1989.

4. A. V. Shevchenko, L. M. Lopato and Z. A. Zaitseva, Russian Journal of Inorganic Materials, 20, 1316 (1984).

5. A. V. Shevchenko, L. M. Lopato and L. V. Nazarenko, Russian Journal of Inorganic Materials, 20, 1615 (1984).

6. S. L. Dole and O. Hunter,Jr., J. Amer. Ceram. Soc., 66, C-47 (1983).

7. E. L. Courtright, Battelle Pacific Northwest Laboratories, private communication, 1990.

8. R. J. Kerans and K. T. Faber, Low Thermal Expansion Coatings for Carbon-Carbon Composites", NASA Conf. Pub. 2482, Metal Matrix, Carbon, and Ceramic Matrix Composites, 1987, 409-425.

9. V. C. Nardone and K. M. Prewo, Scriptamet.,20, 43 (1986).

10. R. J. Kerans et.al. Ceramic Bulletin, 68, 429 (1989).

11. A. G. Evans and D. B. Marshall, Acta Met., 37, 2567 (1989).

12. M. D. Thoulass and A. G. Evans, Acta Met., 36, 517 (1988).

13. M. Pourbaix, "Atlas of Electrochemical Equilibria in Solu tions", NACE, Houston, TX 1974.

14. P. Crocker and B. McEnany, Carbon, 29, 881 (1991).

15. N. A. Saltykova, A. N. Baraboshkin, S. N. Katovskii and A. B. Smirov, Zasch. Met. 14, 228 (1978).

16. G. A. Conn, Plating, 52, 1258 (1965).

17. C. J. Tyrrell, Trans. Inst. Metal Finishing, 43, 161 (1965).

18. E. L. McNamara, J. Electrochem. Soc., 109, 61 (1962).

19. M. R. Nadler and C. P. Kempter, J. Phys. Chem., 64, 1468 (1960).

7. ACKNOWLEDGEMENT

We wish to thank E. L. Courtright of Pacific Northwest Laboratories for valuable discussions of coating strain during thermal cycling of the CAFRIB layer.